Graphene-based biosensors for detection of bacteria and their metabolic activities

Huang, Yinxi; Dong, Xiaochen; Liu, Yuxin; Li, Lain-Jong; Chen, Peng

2011

Huang, Y., Dong, X., Liu, Y., Li, L. J., & Chen, P. (2011). Graphene-based biosensors for detection of bacteria and their metabolic activities. Journal of Materials Chemistry, 21, 12358–12362.

https://hdl.handle.net/10356/94375

https://doi.org/10.1039/c1jm11436k

Graphene-based biosensors for detection of bacteria and their metabolic activities

Yinxi Huang[#a], Xiaochen Dong[#b], Yuxin Liu[a], Lain-Jong Li[c], and Peng Chen[a]*

[a] Division of Bioengineering, School of Chemical and Biomedical Engineering, Nanyang Technological University, 70 Nanyang Drive, Singapore 637457

[b] Key Laboratory for Organic Electronics & Information Displays and Institute of Advanced Materials, Nanjing University of Posts and Telecommunications, 9 Wenyuan Road, Nanjing 210046, China

[c] Research Center for Applied Sciences, Academia Sinica, Taipei 11529, Taiwan

# these authors made equal contribution to this work

*Correspondence: chenpeng@ntu.edu.sg

Table of contents entry:

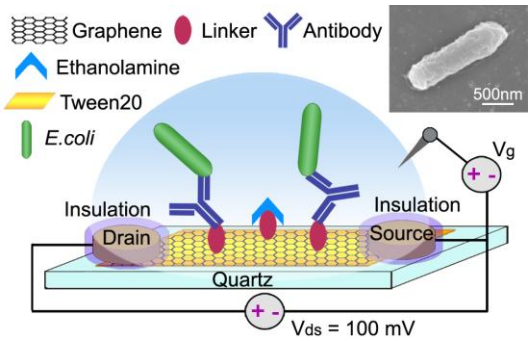

Graphene based nanoelectronic biosensors are applied to detect E. *coli* and its glucose induced metabolic activities.

Abstract

Graphene, which is a recently discovered single-atom-thick planar sheet of carbon atoms perfectly arranged in a honeycomb lattice, has great potential in biosensing owing to its extraordinary electrical, physical, and optical properties. In this work, we demonstrate a graphene based biosensor to electrically detect *E. coli* bacteria with high sensitivity and specificity. The large-sized graphene film was grown by chemical vapor deposition and functionalized with Anti-*E. coli* antibodies and passivation layer. Significant conductance increase of the graphene device was observed after exposure to *E. coli* bacteria at a concentration as low as 10 cfu/mL, while no significant response was triggered by high concentration of the another bacterial strain. In addition, this biosensor was employed to detect the glucose induced metabolic activities of the bound *E. coli* bacteria in real time. This simple, fast, sensitive, and label-free nanoelectronic biosensor, in principle, could serve as a high throughput platform for detection of any pathogenic bacteria, and for functional studies or screening of antibacterial drugs.

Introduction

In the past decade, nanostructured materials have brought great opportunities for biosensing owing to their unique electrical, physical, and optical properties. Especially, various novel nanoelectronic biosensors have been developed based on nanowires [1-5], carbon nanotubes [6-10], and very recently graphene [11-13]. Single-walled carbon nanotubes [14] configured as field-effect transistors (FETs) have recently been used to detect the presence of bacteria. Vallamizar et al. have developed a SWCNT-network FET to detect *S. Infantis* with a sensitivity of 100 cfu/mL [15].

So and colleagues reported a bacteria biosensor based on aptamer-functionalized SWCNT-network FET, which could detect 10^3 cfu/mL *E. coli* [16]. Mulchandani and co-works have demonstrated SWCNT-network based biosensors to electrically detect human pathogen *E. coli* O157:H7 and bacteriophage T7 with a detection limit of 10^3 cfu/mL and 10^3 pfu/mL, respectively [17]. In comparison with the current methods (specifically, the traditional culturing and colony counting method, the polymerase chain reaction method, and the enzyme-linked immunosorbant assay) which are tedious and time consuming (typically taking hours to days), the nanoelectronic approach offers rapid and sensitive measurement.

The recently discovered flat cousin of SWCNT, graphene, which is a single-atom-thick sheet of carbon atoms arranged in a honeycomb structure, has been anticipated as a novel or better alternative to SWCNT in both electrochemical [18, 19] and electronic [20] biosensing, owing to its extraordinary structural, electrical, physical, optical and biocompatible properties [14, 21-23]. For example, its perfect two-dimensional (2D) structure provides large detection area and enables facile and homogeneous functionalization. And the exceptional electrical properties of graphene (such as, high charge mobility and capacity, highly tunable conductance) endow it as an ideal sensing element in electronic sensors [24, 25]. Nanoelectronic biosensors based on graphene have been used for detecting gas molecules [26, 27], metal ions [28], and various biomolecules including DNA [29, 30], glucose [31], and proteins [12, 32, 33]. Mohanty and Berry have presented a FET-sensor with a small patch (a few micrometers) of chemically derived graphene sheet as the sensing element, which is able to detect binding of single bacterium (Gram-positive *Bacillus cereus*) [11]. Although this proof-of-concept study demonstrates the impressive ability of graphene FET for bacteria detection, it is not practical because the detection relied on non-specific electrostatic

adhesion of bacteria without discrimination of bacterial species and the measurement was conducted in dry nitrogen atmosphere.

Here, we demonstrate a nanoelectronic sensor based on antibody-modified chemical-vapor-deposition-grown large-sized graphene to detect bacteria (*E. coli*) with high sensitivity (10 cfu/mL) and specificity. Furthermore, the glucose triggered metabolic activities of bacteria can be detected in real-time. Such simple nanoelectronic biosensor could be useful for rapid and label-free detection of bacteria, high throughput assay of their metabolic activities, and high throughput screening of antibacterial drugs.

Experimental Section

Growth of graphene film and characterizations

Large-sized graphene films were grown on copper foils (Alfa Aestar) by chemical vapor deposition (CVD) using ethanol as the carbon source. Copper foils were loaded into a quartz tubular furnace, which was then purged with pure Ar (1000 sccm) for 10 minutes. After raising the furnace temperature to 900^{o}C, the CVD growth of graphene was started by directing H_2/Ar gas mixture (20% H_2; 40 sccm) with ethanol vapor into the furnace at 900^{o}C. The growth continued for about 30 minutes, following by cooling down under the H_2/Ar atmosphere.

The morphology of graphene surface was characterized with tapping mode atomic force microscopy (AFM) (Dimension3100, Veeco). Raman spectra were obtained with confocal Raman microscopy using a laser wavelength of 488 nm (WITec CRM200).

Fabrication of graphene device

The as-grown graphene film on copper foil was spin-coated with a thin layer of poly-methyl methacrylate (PMMA) dissolved in chlorobenzene, followed by annealing at 180 °C for 1 min. The PMMA/graphene films were then released from the copper foil by chemical etching of the underlying Cu in an iron chloride solution. The suspended film was transferred to DI water to remove the residual copper etchant and then picked up by the substrate. After the PMMA film was dissolved by acetone, the sample was rinsed with copious DI water and annealed at 450 °C for 20 min (H_2/Ar atmosphere). Two electrodes (source and drain) were subsequently prepared cross the graphene film (~2×4 mm^2) using silver conductive paint (RS Component). Finally, silicone rubber (Dow Corning) was used to insulate the electrodes and form the recording chamber.

Functionalization of graphene device

Graphene device was incubated with 5 mM linker molecule (1-pyrenebutanoic acid succinimidyl ester, i-DNA Biotechnology) in dimethylformamide (DMF) for 2 h at room temperature, and washed with pure DMF and DI water. The linker-modified graphene was then incubated with 50 ppm anti-*E. coli* O & K antibody (i-DNA Biotechnology) in Na_2CO_3-$NaHCO_3$ buffer solution (pH 9.0) overnight at 4°C, followed by rinsing with DI water and phosphate buffered saline solution (PBS). Then, the device was incubated with 0.1 M ethanolamine (pH 9.0) for 1 h to quench the unreacted succinimidyl ester group on linker molecules, followed by 1 h incubation with 0.1% Tween 20 to passivate uncoated graphene area.

Preparation of bacteria

E. coli K12 ER2925 purchased from New England Biolab was cultured overnight in Luria Bertani (LB) medium at 37 °C. The harvested *E. coli* solution with addition of 30% glycerol was stored at -80°C as the stock. The density of the *E. coli* stock was determined to be 10^7 cfu/mL using culturing and colony counting method. The stock was diluted in PBS solution (pH 7.2) to produce the desired final concentration of *E. coli* for experiments. Another type of bacteria (*P. aeruginosa*) was similarly prepared for control experiments.

Electrical measurements

All measurements were conducted under ambient conditions using a semiconductor device analyzer (Agilent, B1500A). The graphene device was biased at 100 mV, and the gate voltage was applied via an Ag/AgCl electrode immersed in the PBS solution on top of the graphene.

Results and discussion

Large-sized graphene films were grown on copper foils at 900 ^{o}C by chemical vapor deposition (CVD) using ethanol as the carbon source. After transferred onto the Si/SiO_2 substrate, graphene films were characterized by Raman spectroscopy. Fig. 1A depicts the 2 dimensional Raman map of a graphene film constructed by plotting the peak width at half height of the 2D band in the Raman spectrum. The brighter islands in the Raman map indicate the few-layered regions while the rest is single-layered graphene. The Raman spectrum taken at a darker spot (indicated by a circle in the Raman map) exhibits the characteristic spectrum of single-layered graphene with a sharp 2D peak and a ratio between 2D and G band (I_{2D}/I_G) of ~4.0 (solid trace in Fig. 1A) [34]. In

contrast, the spectrum in a brighter spot (indicated by a square) exhibits an attenuated 2D band and a low I_{2D}/I_G (~0.5), indicating its few-layered structure (dotted trace). As observed, the graphene film is continuous, uniform, and dominantly single-layered. Fig. 1B presents a typical AFM image of graphene film. Some wrinkles are observed in the AFM image, which may be formed during the cooling stage due to the difference in the thermal expansion coefficients between the metal foil and the graphene film [35]. Also, some impurities (white dots) are seen in the AFM image, which are likely the remains of PMMA resulted from the transfer process.

Graphene transistor devices were fabricated on quartz substrate as described in the Experimental Section. To specifically detect bacteria *E. coli*, anti-*E. coli* antibodies were first immobilized onto graphene film *via* the linker molecules (1-pyrenebutanoic acid succinimidyl ester) whose pyrene group at one end binds to the graphene surface through strong *pi-pi* interaction and the succinimidyl ester group at the other end covalently reacts with the amino group on the antibody (Fig. 2A). To prevent non-specific binding, ethanolamine was applied to quench the unreacted succinimidyl esters on the linker molecules and Tween 20 was used to passivate the uncoated graphene area. The inset of Fig. 2A shows an *E. coli* attached onto the antibody functionalized graphene film. As seen from Fig. 2B, the CVD-grown graphene exhibited the characteristic ambipolar field-effect and each functionalization step led to shift in the transfer curve (drain-source current I_{ds} versus the solution-gate voltage V_g).

The graphene sensor was incubated with 10^5 cfu/mL of *E. coli* to determine kinetics of bacteria binding and the device response. As shown in Fig. 3, the graphene conductance increases with time due to gradual increase in the number of *E. coli* caught by the antibodies on the graphene film. As the graphene FET was operated at the *p*-type region (V_g = 0V), the increase in graphene conductance is due to increased hole density induced by the highly

negatively charged bacterial wall. This is consistent with the previous report [11]. The device response reached the maximum in about 1 h due to saturation of bacteria binding (Fig. 3 inset). The kinetic time constant of bacteria binding (time-dependent device response) was about 10 min. In all subsequent experiments, we used 30 min incubation time which allows the device to achieve 95% of the maximum response. In control experiments, 1 h incubation of 10^5 cfu/mL of *E. coli* did not cause any appreciable conductance change in the devices modified only with linker molecules, ethanolamine and Tween 20, suggesting the essential role of anti-*E. coli* antibodies in the detection.

The functionalized graphene devices were incubated with different concentrations of *E. coli* for 30 min, rinsed thoroughly with PBS solution, and electrically characterized by measuring the I_{ds}–V_{ds} (IV) characteristics while the solution-gate voltage V_g was held at 0 V. Fig. 4A show the IV curves of a graphene device before and after exposure to *E. coli* at a concentration from 0 to 10^5 cfu/mL. The increase in graphene conductance positively scaled with the concentration of bacteria. In comparison, 10^5 cfu/mL *P. aeruginosa* did not cause significant response of anti-*E. coli* antibody functionalized graphene FET, indicating the high specificity of detection (Fig. 4B). The specificity is attributable to the facts that other bacterial strain is not able to bind with the anti-*E. coli* antibodies functionalized on the graphene, and non-specific binding to the graphene surface is prevented by Tween-20 passivation. The statistics of the percentage increase in graphene conductance caused by different concentrations of bacteria is shown in Fig. 4C. As seen, *E. coli* with a concentration as low as 10 cfu/mL can be ambiguously detected. This is several orders lower than the previously reported methods using SWCNT-network FETs [15-17], polymerase chain reaction [36], surface plasmon resonance [37]. Specifically, 10 cfu/mL caused 3.25 ± 0.43% increase in graphene conductance (n = 6 devices) which corresponds to a current

increase of ~1.17 μA at V_{ds} = 0.2 V (significantly higher than the current noise of 0.02 μA). In contrast, high concentration of *P. aeruginosa* (10^5 cfu/mL) only produced 1.02 ± 0.81% increase (n = 6 devices). The transfer curves of graphene device measured before and after incubation with *E. coli* (shown in Fig. 4D) indicate the obvious right-shift of the Dirac point and a conductance increase at V_g = 0V, agreeing with the notion that the negatively charged bacteria increase the hole density in graphene.

It is known that glucose metabolism in bacteria leads to extracellular environment due to release of organic acids (e.g. pyruvic, citric, and lactic acid) [38]. We hypothesized that the discharge of organic acids into the nano-gap between the graphene and the interfacing bacterial surface would alter the local pH and consequently the graphene conductance. Firstly, we verified that our graphene device is indeed highly sensitive to pH (Fig. 5). Decrease in pH reduces the graphene conductance. This is consistent with the previous report on single-layer graphene [39].

Anti-*E. coli* antibody functionalized graphene FET was incubated with *E. coli* suspension (10^5 cfu/mL) for 30 min, followed by PBS rinse. As anticipated, decrease of I_{ds} was observed when glucose was added to the recording chamber (Fig. 6). The magnitude of device response is proportional to the glucose concentration (Fig. 6 upper inset) and glucose was not able to trigger any response from a graphene device without bacteria (Fig. 6 lower inset). These observations suggest that the observed signals were resulted from the glucose-induced bacterial metabolism.

Conclusions

In summary, we have developed a fast, label-free, highly sensitive and selective graphene-based biosensor for detection of bacteria *E. coli*. A low detection limit of 10 cfu/mL can be achieved.

Equipped with specific recognition elements, other pathogens may be similarly detected for diagnosis and food or environmental monitoring.

Nanoelectronic biosensos based on one-dimensional semiconducting nanomaterials [40, 41] have been interfaced with mammalian cells to detect their dynamic activities [42-45]. Here, we demonstrated that nanoelectronic sensors based on two-dimensional graphene can be used to detect the metabolic activities of bacteria in real time, providing a high throughput platform for functional studies or for screening of antibacterial drugs.

Acknowledgments

We acknowledge the financial supports from Singapore A*Star SERC grant (#072 101 0020), China NNSF grant (50902071, 61076067, 61006007), China 973 Program (2009CB930601), the Science Foundation of Nanjing University of Posts and Telecommunications (NY208058).

References:

1. F. Patolsky, G. Zheng and C. M. Lieber, Nanomedicine, 2006, 1, 51-65.

2. E. Stern, J. F. Klemic, D. A. Routenberg, P. N. Wyrembak, D. B. Turner-Evans, A. D. Hamilton, D. A. LaVan, T. M. Fahmy and M. A. Reed, Nature, 2007, 445, 519-522.

3. T. S. Pui, A. Agarwal, F. Ye, N. Balasubramanian and P. Chen, Small, 2009, 5, 208-212.

4. T. S. Pui, A. Agarwal, F. Ye, Y. X. Huang and P. Chen, Biosens. Bioelectron., 2011, 26, 2746-2750.

5. K. I. Chen, B. R. Li and Y. T. Chen, Nano Today, 2011, 6, 131-154.

6. G. Gruner, Anal. Bioanal. Chem., 2006, 384, 322-335.

7. B. L. Allen, P. D. Kichambare and A. Star, Adv. Mater., 2007, 19, 1439-1451.

8. Y. X. Huang, P. V. Palkar, L. J. Li, H. Zhang and P. Chen, Biosens. Bioelectron., 2010, 25, 1834-1837.

9. H. G. Sudibya, J. M. Ma, X. C. Dong, S. Ng, L. J. Li, X. W. Liu and P. Chen, Angew. Chem. Int. Ed., 2009, 48, 2723-2726.

10. S. Sorgenfrei, C. Y. Chiu, R. L. Gonzalez, Y. J. Yu, P. Kim, C. Nuckolls and K. L. Shepard, Nat. Nanotechnol., 2011, 6, 125-131.

11. N. Mohanty and V. Berry, Nano Lett., 2008, 8, 4469-4476.

12. Y. Ohno, K. Maehashi and K. Matsumoto, J. Am. Chem. Soc., 2010, 132, 18012-18013.

13. P. K. Ang, M. Jaiswal, C. Lim, Y. Wang, J. Sankaran, A. Li, C. T. Lim, T. Wohland, O. Barbaros and K. P. Loh, Acs Nano, 2010, 4, 7387-7394.

14. S. Agarwal, X. Z. Zhou, F. Ye, Q. Y. He, G. C. K. Chen, J. Soo, F. Boey, H. Zhang and P. Chen, Langmuir, 2010, 26, 2244-2247.

15. R. A. Villamizar, A. Maroto, F. X. Rius, I. Inza and M. J. Figueras, Biosens. Bioelectron., 2008, 24, 279-283.

16. H. M. So, D. W. Park, E. K. Jeon, Y. H. Kim, B. S. Kim, C. K. Lee, S. Y. Choi, S. C. Kim, H. Chang and J. O. Lee, Small, 2008, 4, 197-201.

17. C. Garcia-Aljaro, L. N. Cella, D. J. Shirale, M. Park, F. J. Munoz, M. V. Yates and A. Mulchandani, Biosens. Bioelectron., 2010, 26, 1437-1441.

18. S. Alwarappan, A. Erdem, C. Liu and C. Z. Li, J. Phys. Chem. C, 2009, 113, 8853-8857.

19. S. Alwarappan, C. Liu, A. Kumar and C. Z. Li, J. Phys. Chem. C, 2010, 114, 12920-12924.

20. W. R. Yang, K. R. Ratinac, S. P. Ringer, P. Thordarson, J. J. Gooding and F. Braet, Angew. Chem. Int. Ed., 2010, 49, 2114-2138.

21. A. K. Geim, Science, 2009, 324, 1530-1534.

22. Y. W. Zhu, S. Murali, W. W. Cai, X. S. Li, J. W. Suk, J. R. Potts and R. S. Ruoff, Adv. Mater., 2010, 22, 3906-3924.

23. M. J. Allen, V. C. Tung and R. B. Kaner, Chem. Rev., 2010, 110, 132-145.

24. A. H. Castro Neto, F. Guinea, N. M. R. Peres, K. S. Novoselov and A. K. Geim, Rev. Mod. Phys., 2009, 81, 109-162.

25. C. Riedl, C. Coletti and U. Starke, J. Phys. Appl. Phys., 2010, 43.

26. G. H. Lu, L. E. Ocola and J. H. Chen, Nanotechnology, 2009, 20.

27. Q. M. Ji, I. Honma, S. M. Paek, M. Akada, J. P. Hill, A. Vinu and K. Ariga, Angew. Chem. Int. Ed., 2010, 49, 9737-9739.

28. H. G. Sudibya, Q. Y. He, H. Zhang and P. Chen, ACS nano, 2011, 5, 1990-1994.

29. X. C. Dong, Y. M. Shi, W. Huang, P. Chen and L. J. Li, Adv. Mater., 2010, 22, 1649-1653.

30. R. Stine, J. T. Robinson, P. E. Sheehan and C. R. Tamanaha, Adv. Mater., 2010, 22, 5297-5300.

31. Y. X. Huang, X. C. Dong, Y. M. Shi, C. M. Li, L. J. Li and P. Chen, Nanoscale, 2010, 2, 1485-1488.

32. S. Mao, G. H. Lu, K. H. Yu, Z. Bo and J. H. Chen, Adv. Mater., 2010, 22, 3521-3526.

33. Q. Y. He, S. X. Wu, S. Gao, X. H. Cao, Z. Y. Yin, H. Li, P. Chen and H. Zhang, ACS nano, 2011, DOI: 10.1021/nn201118c.

34. Z. H. Ni, H. M. Wang, J. Kasim, H. M. Fan, T. Yu, Y. H. Wu, Y. P. Feng and Z. X. Shen, Nano Lett., 2007, 7, 2758-2763.

35. S. J. Chae, F. Gunes, K. K. Kim, E. S. Kim, G. H. Han, S. M. Kim, H. J. Shin, S. M. Yoon, J. Y. Choi, M. H. Park, C. W. Yang, D. Pribat and Y. H. Lee, Adv. Mater., 2009, 21, 2328-2333.

36. A. D. Taylor, J. Ladd, Q. M. Yu, S. F. Chen, J. Homola and S. Y. Jiang, Biosens. Bioelectron., 2006, 22, 752-758.

37. Y. X. Wang, Z. Z. Ye, C. Y. Si and Y. B. Ying, Sensors, 2011, 11, 2728-2739.

38. M. Solé, N. Rius and J. G. Lorén, Int. Microbiol., 2000, 3, 39-43.

39. Y. Ohno, K. Maehashi, Y. Yamashiro and K. Matsumoto, Nano Lett., 2009, 9, 3318-3322.

40. A. Noy, A. B. Artyukhin and N. Misra, Mater. Today, 2009, 12, 22-31.

41. Y. X. Huang and P. Chen, Adv. Mater., 2010, 22, 2818-2823.

42. F. Patolsky, B. P. Timko, G. H. Yu, Y. Fang, A. B. Greytak, G. F. Zheng and C. M. Lieber, Science, 2006, 313, 1100-1104.

43. Y. X. Huang, H. G. Sudibya, D. L. Fu, R. H. Xue, X. C. Dong, L. J. Li and P. Chen, Biosens. Bioelectron., 2009, 24, 2716-2720.

44. T. S. Pui, A. Agarwal, F. Ye, Z. Q. Ton, Y. X. Huang and P. Chen, Nanoscale, 2009, 1, 159-163.

45. T. S. Pui, H. G. Sudibya, X. N. Luan, Q. Zhang, F. Ye, Y. X. Huang and P. Chen, Adv. Mater., 2010, 22, 3199-3203.

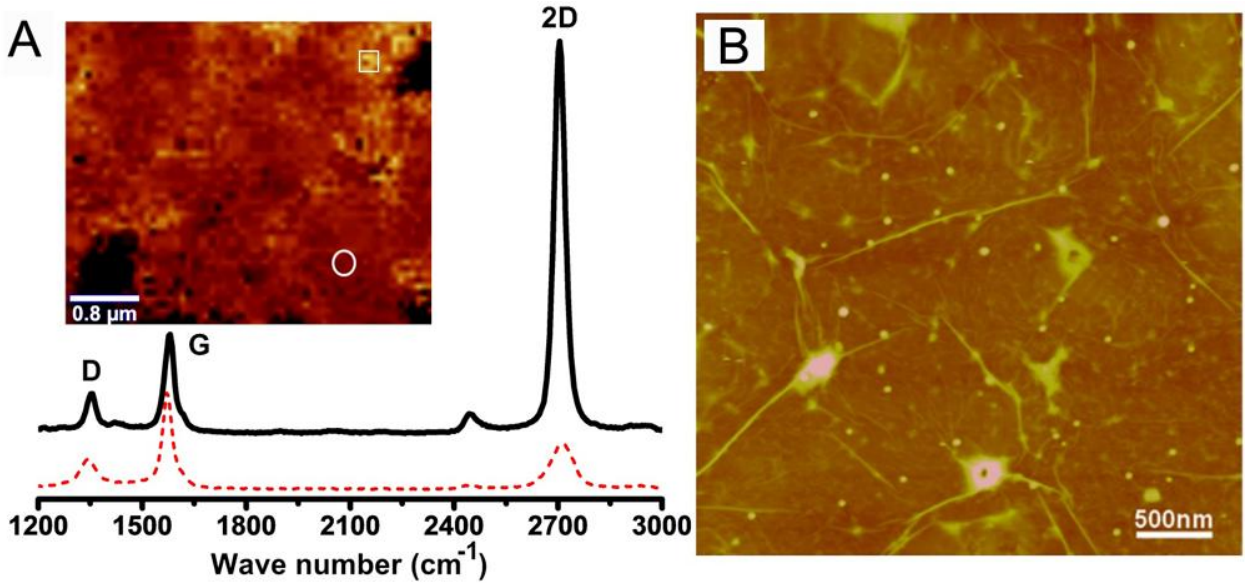

Fig. 1 (A) Raman map and spectrum of graphene film. The map is constructed by plotting the peak width at half height of the 2D-band as the pixel intensity. Scale bar = 0.8 μm. (B) AFM image of the graphene film. Scale bar = 500 nm.

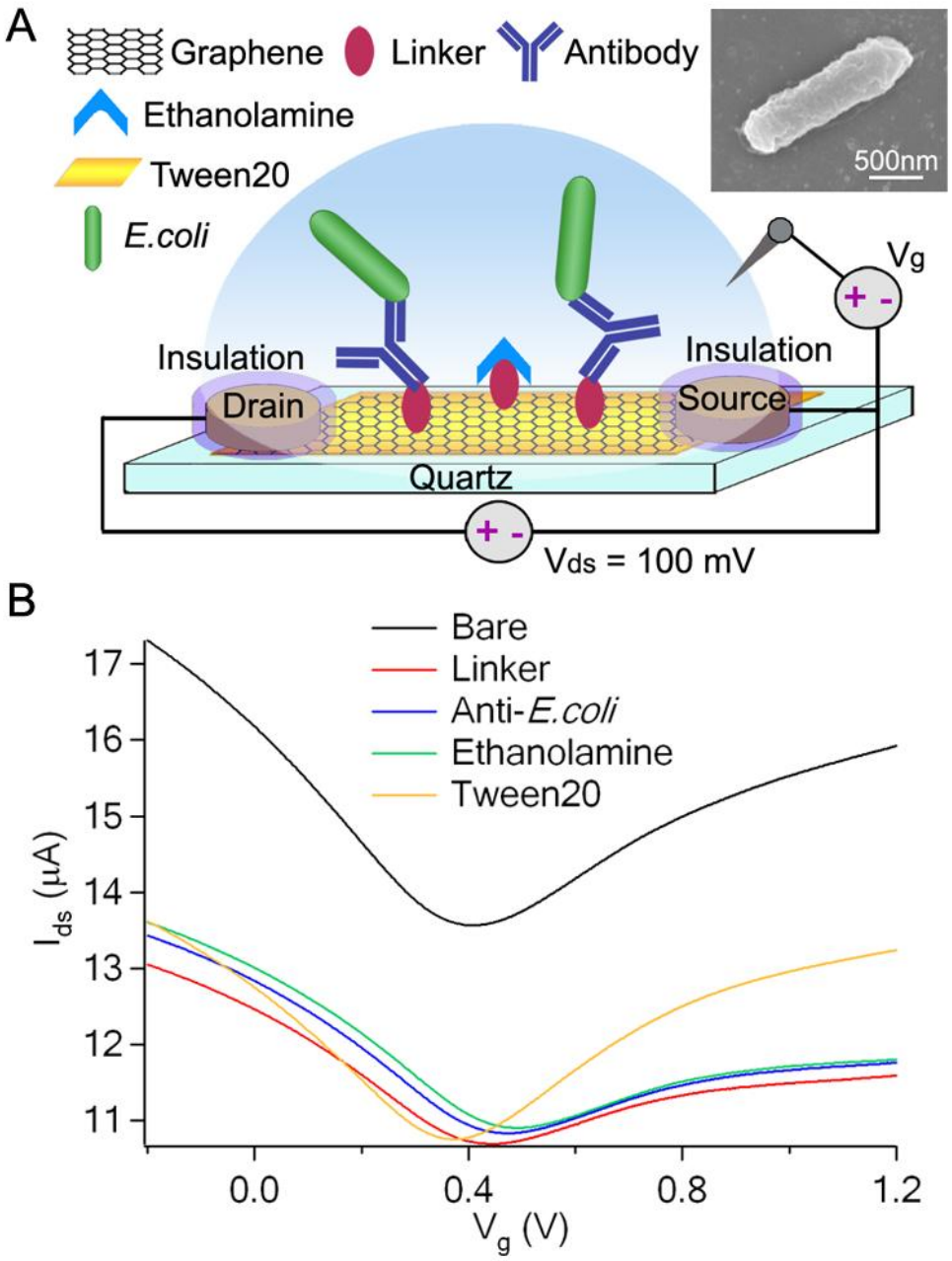

Fig. 2 A) Illustration of anti-*E. coli* antibody functionalized graphene-FET for detection of *E. coli*. Inset: Scanning electron microscopy (SEM) image of an *E. coli* on antibody functionalized graphene. B) Transfer curves of a graphene FET before functionalization and after functionalizing sequentially with linker molecules, anti- *E. coli* antibodies, ethanolamine and Tween 20. V_{ds}=100mV.

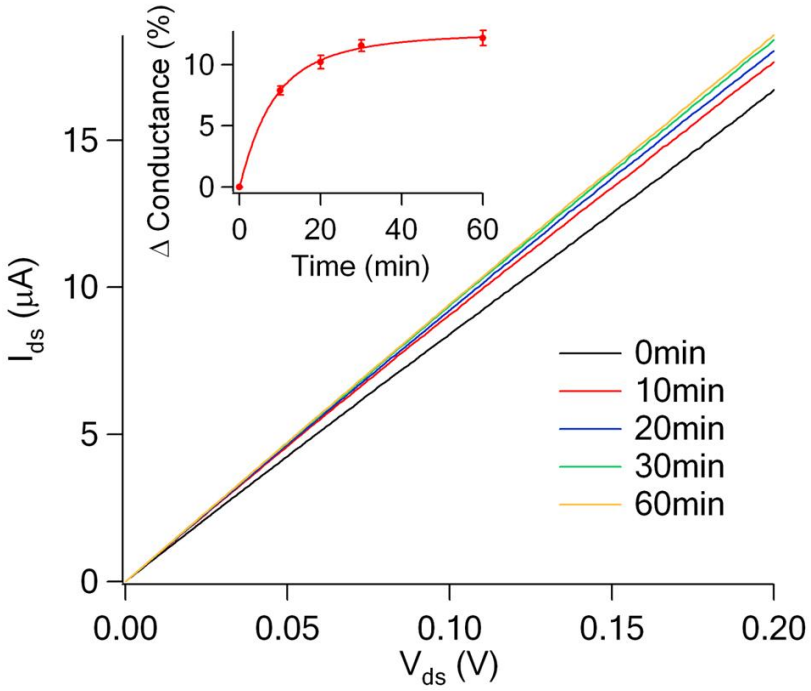

Fig. 3 Transfer curves of graphene FET in buffer solutions with different pH values (pH 3, 5, 7, 9 and 11). V_{ds}=100mV; V_g=0V. Inset: Dirac point of graphene device over pH values. Each data point is the average from 3 devices. The error bars indicate the standard errors.

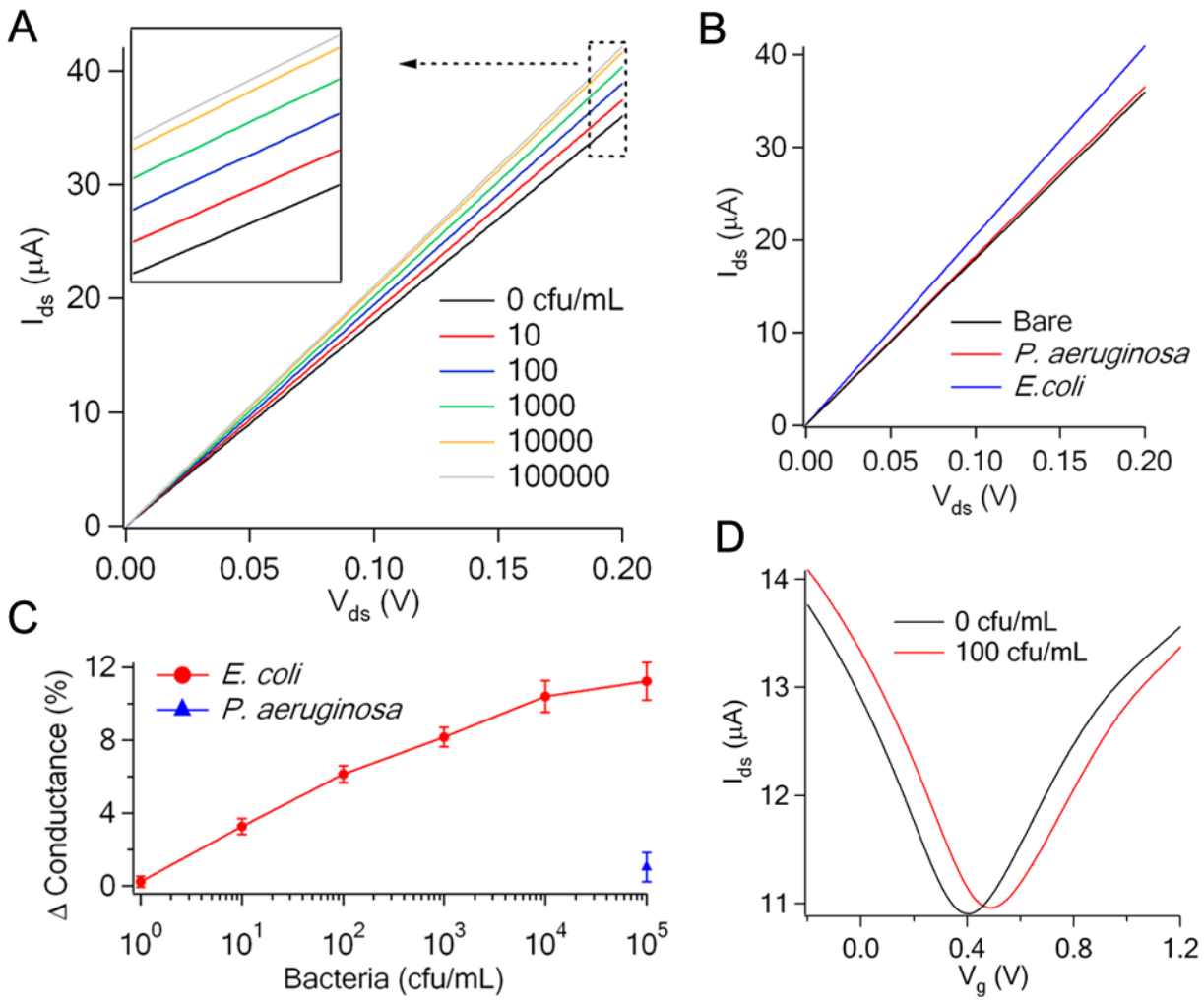

Fig. 4 A) I_{ds} versus V_{ds} curves of anti-*E. coli* antibody functionalized graphene device after incubated with *E. coli* of different concentrations. V_g=0V. B) I_{ds} versus V_{ds} curves of antibody functionalized graphene device before and after incubated with *P. aeruginosa* and *E. coli* (both 10^5 cfu/mL). V_g = 0V. C) Percentage change of graphene conductance caused by *P. aeruginosa* (triangle) and *E. coli* (circles) of different concentrations. Each data point is the average from 6 devices. The error bars indicate the standard errors. D) Transfer curves of antibody functionalized graphene FET before and after incubation with *E. coli* (100 cfu/mL). V_{ds}=100mV.

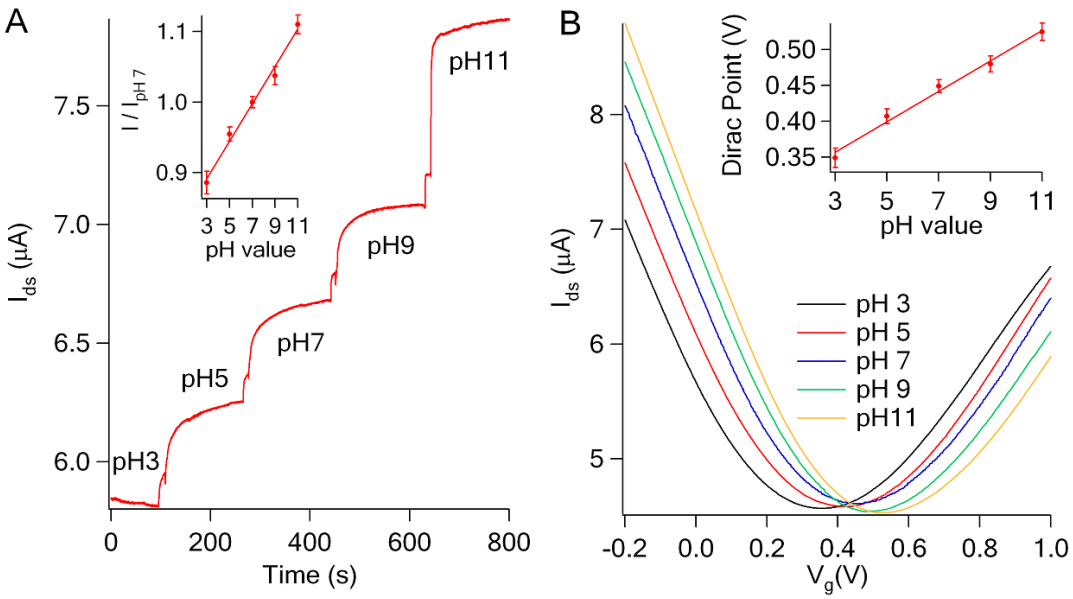

Fig. 5 A) Real-time current of graphene device while changing solutions with different pH values (pH 3, 5, 7, 9 and 11). V_{ds}=100mV; V_g=0V. Inset: Percentage change of graphene conductance over pH values. Each data point is the average from 3 devices. The error bars indicate the standard errors. B) Transfer curves of graphene FET in buffer solutions with different pH values (pH 3, 5, 7, 9 and 11). V_{ds}=100mV; V_g=0V. Inset: Dirac point of graphene device over pH values. Each data point is the average from 3 devices. The error bars indicate the standard errors.

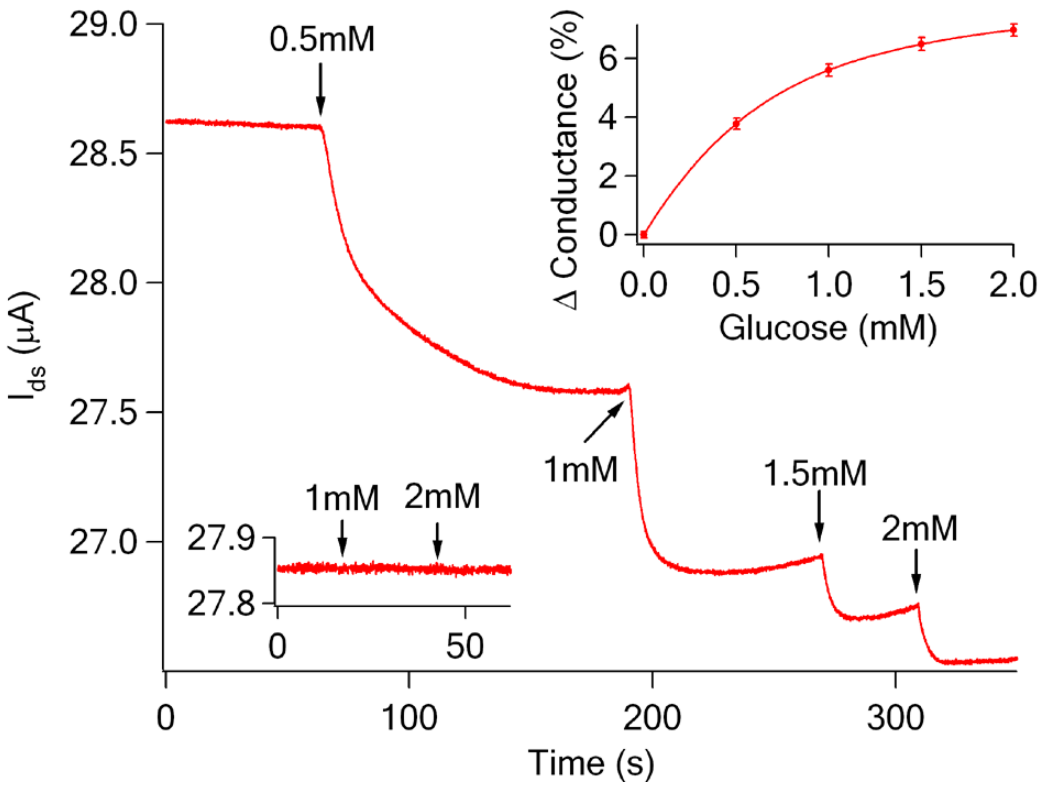

Fig. 6 Real-time current recording (V_{ds} = 100 mV and V_g = 0 V) of a graphene device immobilized with *E. Coli* bacteria (incubated with 10^5 cfu/mL *E. coli* for 30 min followed by rinsing), with application of glucose to the PBS recording buffer at the indicated time points to reach the final concentrations of 0.5, 1, 1.5, and 2 mM. Lower inset: bacteria free graphene sensor was not responsive to glucose. Upper inset: Percentage change in graphene conductance versus glucose concentration. Each data point is the average from 3 devices. The error bars indicate the standard errors.